Vol. 04, Iss. 3 (2026) 378-387, DOI: 10.61552/JME.2026.03.007

Journal of Materials and Engineering

www.jme.aspur.rs

Research article

Impact of Chromium Nitride (CrN) Coating Deposited by PVD Technique on the Fatigue Behavior of Case Carburized SAE8620 Grade Steel

Kumar Sushil[a,*], Saini Balraj[a]

[a]*Mechanical Engineering Department, Punjabi University, India.*

Keywords:

Fatigue
SAE8620
Chromium Nitride
PVD coating
S-N curve
Endurance limit

* Corresponding author:

Kumar Sushil
E-mail: sushilgargiitd@gmail.com

Received: 17 July 2026
Revised: 21 August 2026
Accepted: 7 September 2026

A B S T R A C T

The fatigue performance of case-carburized SAE8620 steel with and without a Physical Vapour Deposition (PVD) chromium nitride (CrN) coating was investigated under four-point rotating bending. Cylindrical specimens were carburized, oil quenched, tempered and subsequently polished to obtain a surface hardness of 60-62 HRC. Half of the specimens were then coated with an approximately 2 µm thick CrN layer using an ion-sputtering PVD process. Fatigue tests were carried out at different stress amplitudes in accordance with ASTM E739 (2015), and the resulting stress-life (S-N) behaviour was compared using fitted regression curves because the coated and uncoated series were tested at different stress levels. The mean endurance limits determined using the Dixon-Mood staircase method were 770 MPa for the uncoated specimens and 657.5 MPa for the coated specimens. Fractographic examination showed coating-associated crack origins in the coated condition and isolated surface discontinuities in the uncoated condition. The observed fatigue-strength reduction may be associated with coating defects, interfacial effects and elastic mismatch; residual stress and adhesion were not measured directly. Within the experimentally investigated life range, a Basquin-based coating knockdown factor, $K(N) \approx 1.33N^{-0.032}$, indicates an increasing strength penalty with cycle number. Benchmarking against a companion CrN-coated 20MnCr5 dataset further indicates that the magnitude of the fatigue penalty is substrate-dependent. These results show that the fatigue consequences of CrN coating should be assessed separately from its established surface-engineering benefits.

1. INTRODUCTION

SAE8620 is low-alloy carburizing steel that is extensively used for manufacturing gears, shafts and other rotating transmission components because of its good combination of strength, tough-ness and wear resistance [1]. During service, these components are simultaneously subjected to cyclic loading and sliding contact, making fatigue and wear the dominant failure mechanisms. Im-proving fatigue resistance while maintaining excellent surface durability is therefore an important objective in the design of automotive and aerospace components.

Case carburization is one of the most widely adopted surface hardening treatments for SAE8620 steel. The process produces a hard, wear-resistant surface supported by a relatively tough core and also introduces beneficial compressive residual stresses near the surface, which delay fatigue crack initiation and improve fatigue life [2-7]. More recently, the combined influence of thermal treatment parameters and surface roughness on the fatigue response of SAE8620 steel has also been investigated [8]. Consequently, carburized SAE8620 steel has become a preferred material for components operating under repeated bending and contact loading.

Besides heat treatment, thin hard coatings deposited by Physical Vapour Deposition (PVD) and Chemical Vapour Deposition (CVD) have been increasingly applied to improve the surface charac-teristics of engineering components. Such coatings reduce friction, improve wear resistance and increase corrosion resistance without significantly altering the bulk properties of the substrate [9]. Several studies have also reported improvements in fatigue performance after deposition of TiN and related ceramic coatings on selected engineering alloys [10-13]. However, the fatigue re-sponse depends strongly on coating composition, coating integrity, residual stresses developed during deposition and the mechanical compatibility between the coating and the substrate.

Among the commercially available PVD coatings, chromium nitride (CrN) has attracted considera-ble attention because of its high hardness, good adhesion, excellent oxidation resistance and com-paratively lower deposition temperature. These characteristics make CrN particularly suitable for heat-treated steels, where excessive temperatures during the coating process can reduce the hardness achieved though carburization. Previous investigations have mainly focused on the tribological behaviour and wear resistance of CrN coatings, while comparatively fewer studies have examined their influence on the fatigue behaviour of carburized low-alloy steels. A recent study by Kumar and Saini on case-carburized 20MnCr5 steel demonstrated that an approximately 2 μm PVD CrN coating can reduce the fatigue endurance limit, emphasizing that the fatigue re-sponse of CrN-coated carburizing steels must be assessed independently of their tribological ben-efits [14].

The present work investigates the influence of a PVD-deposited CrN coating on the fatigue behav-iour of case-carburized SAE8620 steel under four-point rotating bending. Fatigue lives, S–N char-acteristics and endurance limits of coated and uncoated specimens are compared using identical testing conditions. Fractographic observations are further used to identify the dominant crack ini-tiation and propagation mechanisms responsible for the observed fatigue behaviour. The findings provide useful information for selecting surface engineering treatments for fatigue-critical com-ponents used in automotive and aerospace applications.

The novelty of the present study lies in isolating the fatigue response of a hard ceramic CrN coat-ing on case-carburized SAE8620 and placing it in direct context with the authors' earlier coated-carburized-steel studies. The earlier SAE8620 work used a mechanically distinct WC/C coating [15], whereas the companion CrN study used a different carburizing substrate, 20MnCr5 [14]. By retaining SAE8620 while changing the coating system, and separately retaining CrN while chang-ing the substrate, the present work enables two complementary comparisons: coating-system sensitivity on the same substrate and substrate sensitivity for nominally the same coating. The present analysis further quantifies the CrN effect through fitted S-N relations, a life-dependent knockdown factor, Dixon-Mood endurance limits and fractographic observations. This combina-tion provides a substrate-resolved assessment of CrN-related fatigue degradation rather than a routine extension of the earlier studies.

2. EXPERIMENTAL PROCEDURE

2.1 Material and specimen preparation

2.1.1 Material selection

Commercial SAE8620 low-alloy carburizing grade steel was selected for the present investigation because of its extensive application in gears, shafts and other rotating components used in automotive and aerospace systems. The steel offers a favourable combination of strength, toughness and hardenability after case carburization. The chemical composition of the material, determined by optical emission spectroscopy, is listed in Table 1. The principal alloying elements include chromium, nickel and molybdenum, which contribute to the hardenability and mechanical response of the carburized steel [1,5].

Table 1. Alloying elements in SAE8620 grade material (weight percentage).

C	Ni	Si	Mn	Cr	Mo
0.18	0.60	0.16	0.72	0.59	0.24

2.1.2 Specimen preparation

Fatigue specimens for four-point rotating bending tests were prepared in accordance with ISO 1143:2021 [16]. The cylindrical specimen geometry is shown in Figure 1 and was selected to provide a uniform stress distribution over the gauge section while minimizing stress-concentration effects.

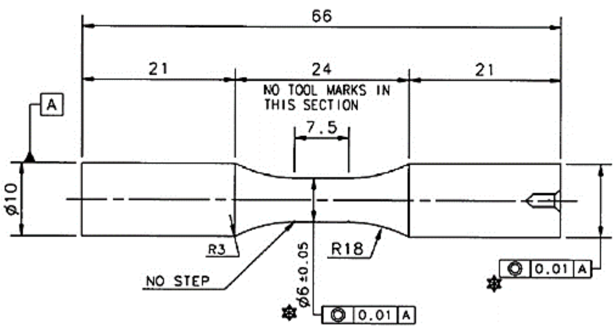

Fig. 1. Test specimen design as per ISO 1143.

All specimens were machined from 14 mm diameter SAE8620 steel bars obtained from the same production heat to ensure uniform chemical composition and metallurgical consistency throughout the investigation. Machining was carried out on a CNC lathe using tungsten carbide cutting tools to achieve the required dimensional accuracy and surface finish.

2.2 Heat Treatment and CrN coating

After machining, the specimens were subjected to case carburization. Austenitization was carried out at 920°C, followed by oil quenching from 850°C and tempering at 180°C. This heat treatment produced a hardened case with a surface hardness in the range of 60–62 HRC.

Following heat treatment, all specimens were ground and polished to obtain a smooth surface suitable for fatigue testing. Mechanical polishing was performed using silicon carbide abrasive papers with grit sizes ranging from 320 to 1400, followed by final polishing with levigated alumina paste. The polished specimens exhibited an average surface roughness of approximately Ra = 0.20 μm. Surface roughness was evaluated in terms of the arithmetic mean roughness, Ra, before and after coating. Additional profilometer settings (instrument model, cutoff/evaluation length and number of traces) are not available in the experimental record used for this manuscript and are therefore not reported. Before coating, the specimens were protected from corrosion by immersion in SAE 20W-40 oil.

A chromium nitride (CrN) coating approximately 2 μm thick was deposited on half of the specimens using an ion-sputtering Physical Vapour Deposition (PVD) process at M/s Oerlikon Balzers, India. Prior to deposition, the specimen surfaces were cleaned by degreasing and ion etching to improve surface cleanliness and coating attachment. The deposition temperature was approximately 220°C, thereby avoiding substantial thermal exposure of the carburized case. The available experimental record does not contain the proprietary chamber pressure, gas-flow, substrate-bias or target-power settings; these parameters are therefore not inferred or reported.

After coating, the measured average surface roughness was approximately Ra = 0.16 μm, compared with approximately Ra = 0.20 μm before coating. CrN was selected as a surface-engineering treatment because such coatings are commonly used for hardness, wear and corrosion-related applications [17,18]; however, wear resistance, corrosion resistance and coating adhesion were not measured in the present fatigue study.

2.3 Metallographic examination

Metallographic analysis was performed to examine the microstructure developed after case carburization and heat treatment. The specimens were sectioned, polished, mounted and etched using standard metallographic procedures for microscopic examination.

The microstructure consisted of a hardened carburized case and a comparatively tougher core. The core region predominantly exhibited lower bainite, which is commonly observed in properly heat-treated SAE8620 steel and contributes to good strength and toughness. The occurrence of bainitic constituents in high-strength steels and lower-bainitic features in carburized SAE8620 is consistent with prior observations [19,15].

2.4 Fatigue testing

Fatigue tests were carried out under four-point rotating bending in accordance with ISO 1143:2021 [16]. The experimental arrangement is shown in Figure 2. This loading configuration provides a constant bending moment over the gauge section, ensuring that fatigue cracks initiate within the uniformly stressed region of the specimen. All tests were performed at a rotational speed of 3000 rpm under laboratory ambient conditions. Fatigue lives were determined by recording the number of cycles to failure at the applied stress levels listed in Tables 2 and 3.

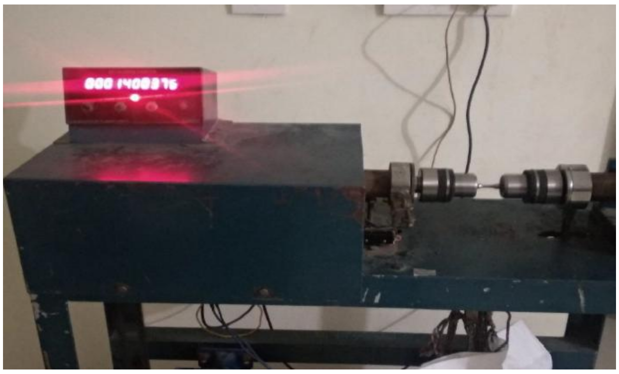

Fig. 2. Fatigue testing experimental setup.

The S-N data were analysed using a log-log linearization of the Basquin relation in accordance with the statistical framework of ASTM E739 (2015) [20]. Two specimens were tested at each stress level. The duplicate results are reported individually in Tables 2 and 3, together with their arithmetic mean and sample standard deviation. The mean life at each stress level was used for the plotted regression. The 95% confidence limits shown in Figure 3 refer to the confidence limits associated with the fitted log-log S-N regressions; they are not additional experimental data points and should not be interpreted as specimen-to-specimen tolerance limits.

Table 2. No. of cycles up to failure (N) v/s applied stress(S) data for specimens in uncoated condition.

Stress (MPa)	Cycle to failure		Average	Std. dev.
	N_1	N_2	$N_f^{uncoated}$	$\sigma^{uncoated}$
970	15350	11768	13559	2533
940	29170	23458	26314	4039
910	68421	45643	57032	16106
880	116792	87658	102725	20601
845	193245	162092	177668	22028
810	435649	289763	362706	103157
780	567546	980795	774170	292211

Table 3. No. of cycles up to failure (N) v/s applied stress(S) data for specimens in coated condition.

Stress (MPa)	Cycle of failure		Average	Std. dev.
	N_1	N_2	N_f^{coated}	σ^{coated}
905	17574	24765	21170	5085
855	40266	63482	51874	16416
815	91759	106540	99150	10452
745	272882	308765	290824	25373
715	374987	412390	393689	26448
670	524754	650840	587797	89156

The endurance limit was estimated separately for coated and uncoated conditions using the Dixon-Mood staircase method [21]. In this up-and-down procedure, the stress level is changed by a fixed increment according to the preceding failure/runout outcome. The stress-level index k and the number of effective events nDM,k are used to calculate the first and second moments ADM and BDM. For the present staircase datasets, the increments were d = 25 MPa for coated specimens and d = 20 MPa for uncoated specimens. The resulting mean endurance limit and estimated standard deviation are reported explicitly in Table 4. Because only a small number of effective staircase reversals were available, these endurance-limit estimates should be interpreted as preliminary statistical estimates rather than high-precision population parameters.

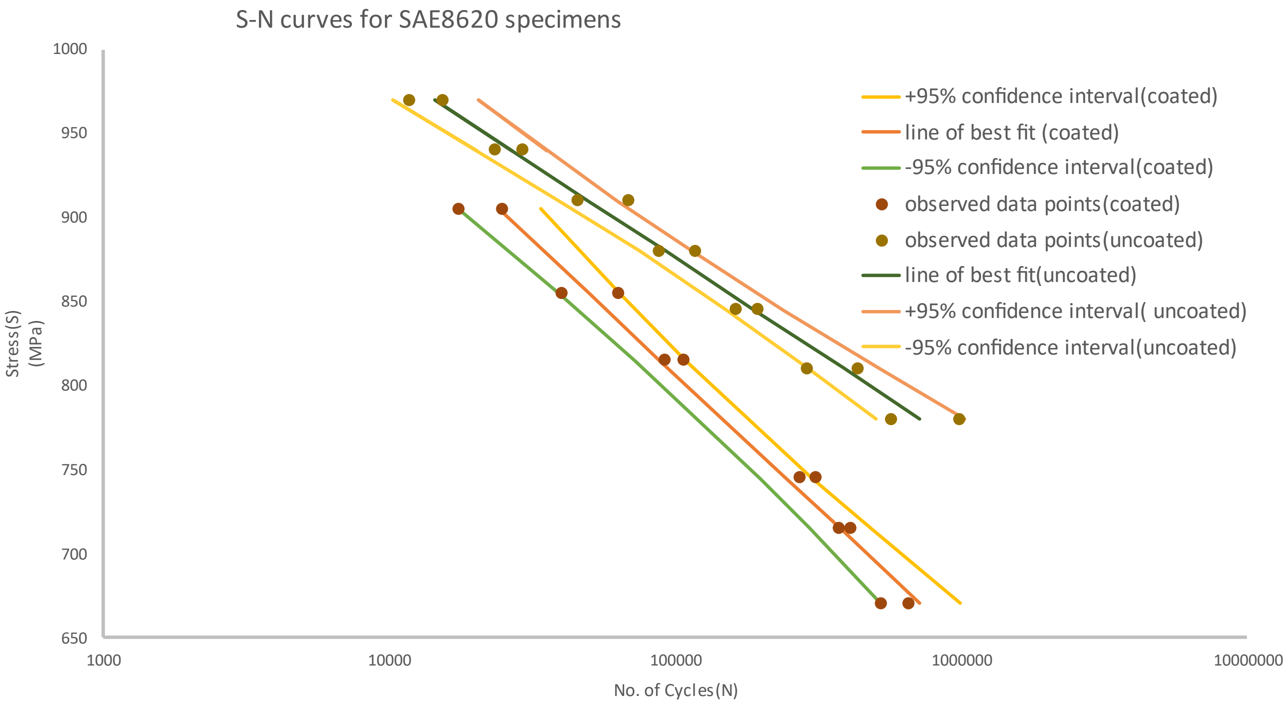

Fig. 3. Stress vs cycles curve for both types of specimens.

3. RESULTS AND DISCUSSION

3.1 Hardness after case carburization

Case carburization followed by quenching and tempering produced a hardened surface layer with a measured hardness of 60–62 HRC. This increase in hardness is attributed to carbon enrichment of the surface during carburization and the subsequent martensitic transformation during quenching. The hardened case is expected to improve wear resistance and delay fatigue crack initiation under cyclic loading.

3.2 Fatigue Behavior

Rotating-bending fatigue data were statistically analysed in accordance with ASTM E739 (2015) [20]. Two specimens were tested at each stress level, and the individual lives, arithmetic means and sample standard deviations are presented in Tables 2 and 3. Because the coated and uncoated series were tested at different stress amplitudes, direct point-by-point comparison at identical stress levels is not possible. Accordingly, the comparative statements below are based primarily on the fitted S-N regression curves over their overlapping experimentally supported life range, with the raw measurements used to establish each fit.

For both the uncoated and CrN-coated specimen conditions, fatigue life increased as stress amplitude decreased, consistent with the expected high-cycle fatigue trend for carburized low-alloy steels. Comparison of the fitted S-N curves shows that, over the overlapping experimentally supported life range, the CrN-coated condition has lower predicted fatigue strength at a given life than the uncoated condition.

The separation between the fitted curves increases toward longer lives within the measured range. This trend suggests that the coating has a stronger influence in the high-cycle region and is consistent with a larger contribution from crack-initiation processes at lower stress amplitudes. This interpretation is supported by the fractographic observations discussed in Section 3.5, but it is not taken as a direct measurement of crack-initiation life.

3.3 Stress–Life (S–N) behavior

Figure 3 compares the fitted S-N curves and 95% regression confidence limits for coated and uncoated SAE8620 specimens. Since different stress levels were used for the two test series, the comparison is made at common fatigue lives from the fitted Basquin relations rather than by pairing individual tests at identical applied stresses. Within the overlapping experimentally supported range, the fitted curve for the uncoated condition lies above that for the CrN-coated condition, and the separation increases toward longer fatigue lives.

To quantify the S–N response, the mean fatigue-life data in Tables 2 and 3 were fitted to the Basquin power-law relationship, $S = AN^b$, using a log–log least-squares regression. For the uncoated specimens the fit gave A ≈ 1652 MPa and b ≈ −0.055 (R^2 = 0.99), while the CrN-coated specimens gave A ≈ 2197 MPa and b ≈ −0.087 (R^2 = 0.98). Both fits describe the experimental data closely over the tested range, and the appreciably steeper fatigue-strength exponent for the coated condition provides a quantitative measure of the greater sensitivity of the coated specimens to cycle number, consistent with the widening separation between the two S–N curves at longer lives noted above.

The two Basquin fits can be combined to obtain a life-dependent coating knockdown factor, K(N) = Scoated(N)/Suncoated(N)=(Acoated/Auncoated)N^(bcoated-buncoated), which expresses the predicted fatigue-strength retention of the coated condition relative to the uncoated condition at a common life. Substitution of the fitted coefficients gives K(N) ≈ 1.33N^-0.032. To avoid unsupported extrapolation, this relation is interpreted only within the experimentally investigated life range. For illustration, K(N) is approximately 0.99 at 10^4 cycles, 0.92 at 10^5 cycles and 0.87 at 5 × 10^5 cycles, corresponding to predicted strength penalties of about 1%, 8% and 13%, respectively. The value at 10^6 cycles previously discussed is outside the coated experimental range and is therefore not used as a quantitative result in the revised manuscript.

A first-order elastic-mismatch estimate was used only as a mechanistic indicator. Reported Young's moduli for PVD CrN coatings span approximately 230-420 GPa depending on deposition conditions and measurement direction, compared with approximately 205-210 GPa for steel substrates [11]. Taking a representative CrN modulus of 300 GPa gives an elastic-mismatch parameter α = (Ecoating-Esubstrate)/(Ecoating+Esubstrate) ≈ 0.18. A positive mismatch of this order is consistent with the possibility of local interfacial stress concentration in a stiff ceramic coating/substrate system [11,12]. This estimate does not constitute a measurement of the coating modulus, residual stress or interfacial stress state in the present specimens; it is used only to support interpretation of the observed coating-associated crack origins.

CrN coatings are widely used for surface-engineering applications, but the present experiments were designed to measure fatigue behaviour rather than wear, corrosion, residual stress or adhesion. The observed reduction in fatigue performance may be associated with the combined influence of local coating imperfections, coating/substrate elastic mismatch and an unmeasured deposition-induced residual-stress state. These mechanisms are therefore presented as plausible interpretations consistent with the fractography and literature, not as directly measured causes.

The present observations are consistent with previous reports that hard ceramic coatings do not necessarily improve fatigue performance when coating-related defects or an unfavourable residual-stress state promote surface crack initiation [8,11-13]. In the present work, however, residual stress and adhesion were not measured directly, so no quantitative attribution to either factor is made.

3.4 Endurance limit

The endurance limits of the two specimen conditions were estimated using the Dixon-Mood staircase method described in Section 2.4 and summarized in Table 4. The mean endurance limit was 770 MPa for the uncoated case-carburized specimens and 657.5 MPa for the CrN-coated specimens, corresponding to a reduction of 14.6%. The estimated standard deviations from the Dixon-Mood calculation were 10.60 MPa and 13.25 MPa, respectively. Given the small number of effective staircase events, these values are reported as preliminary statistical estimates.

Table 4. Results of staircase test data obtained by method of Dixon-Mood statistical analysis.

<table>
<tr><th>k</th><th colspan="2">Coated Case Carburized specimens</th><th colspan="2">Uncoated case carburized specimens</th></tr>
<tr><td>0</td><td>S_0 = 595 MPa</td><td>$n_0 = 0$</td><td>S_0 = 720 MPa</td><td>$n_0 = 0$</td></tr>
<tr><td>1</td><td>S_1 = 620 MPa</td><td>$n_1 = 0$</td><td>S_1 = 740 MPa</td><td>$n_1 = 0$</td></tr>
<tr><td>2</td><td>S_2 = 645 MPa</td><td>$n_2 = 0$</td><td>S_2 = 760 MPa</td><td>$n_2 = 0$</td></tr>
<tr><td>3</td><td>S_3 = 670 MPa</td><td>$n_3 = 2$</td><td>S_3 = 780 MPa</td><td>$n_3 = 2$</td></tr>
<tr><td colspan="3">Stress increased in each step, d(Mpa) = 25
$A_{DM} = \sum(k)\,(n_{DM,k}) = 6$
$B_{DM} = \sum(k^2)\,(n_{DM,k}) = 18$
$\frac{B_{DM}\sum(nk) - A^2_{DM}}{(\sum n_{DM,k})^2}$
= (18*2-36)/4=0 < 0.3
Mean stress, μ_s (MPa)= 595 +25 (6/2 - 0.5) = 657.5
Standard deviation, σ_s (MPa) = 0.53d = 13.25</td><td colspan="2">Stress increased in each step, d(Mpa) = 20
$A_{DM} = \sum(k)\,(n_{DM,k}) = 6$
$B_{DM} = \sum(k^2)\,(n_{DM,k}) = 18$
$\frac{B_{DM}\sum(n_k) - A^2_{DM}}{(\sum n_{DM,k})^2}$
= (18*2-36)/4=0 <0.3
Mean stress, μ_s (MPa) = 720 + 20 (6/2 - 0.5) = 770
Standard deviation, σ_s(Mpa) = 0.53d = 10.60</td></tr>
</table>

The lower staircase endurance limit for the coated condition is consistent with the relative position of the fitted S-N curves, although the two analyses use different parts of the fatigue dataset. Comparison with the companion study of an identically deposited CrN coating on case-carburized 20MnCr5 steel [14] provides additional context: that study reported a decrease from 730 MPa to 687.5 MPa (5.8%), compared with 14.6% for SAE8620 here. Because coating chemistry and nominal thickness were similar while the substrate differed, the comparison indicates that the magnitude of coating-associated fatigue degradation is substrate-sensitive. It does not, by itself, identify the controlling mechanism, since substrate microstructure and near-surface residual stress were not measured comparatively in the present work.

3.5 Fractographic analysis

Fracture surfaces from the uncoated and CrN-coated test series were examined using scanning electron microscopy to identify fatigue-failure features, as shown in Figure 4. The images are used to compare the two surface conditions qualitatively. Specimen-specific applied-stress and cycles-to-failure identifiers for the archived SEM panels are not available in the experimental record used for this manuscript; therefore, no unsupported specimen-level values have been assigned to the images.

The uncoated specimens exhibited characteristic fatigue-fracture features in Figure 4a, including a crack-initiation region, a stable propagation zone and a final overload region. Crack initiation was associated mainly with isolated surface irregularities in the maximum-bending-stress region. The propagation zone contained fatigue striations and occasional secondary cracks, while the final fracture region displayed ductile dimples. In contrast, the coated condition in Figure 4b showed crack origins associated with local coating defects and the coating/substrate interface, together with local microcracking and partial delamination near the origin. These observations support an association between local coating damage and earlier crack nucleation, but they do not provide a direct measurement of adhesion strength or residual stress.

The SEM observations are consistent with the lower fitted fatigue strength and lower staircase endurance limit of the coated condition. They suggest that local coating damage can provide preferential crack-initiation sites under rotating bending. Optimization of coating thickness, deposition conditions and interface quality may therefore be relevant for fatigue-critical use, but the present study did not independently measure adhesion, residual stress, wear performance or corrosion performance.

Several limitations should be acknowledged. Duplicate testing at each S-N stress level provides only limited statistical power, and the Dixon-Mood estimates were derived from a small number of effective staircase events; larger specimen populations would narrow uncertainty. The 95% limits in Figure 3 describe uncertainty associated with the fitted regressions and should not be interpreted as tolerance limits for future specimens. In addition, coating residual stress, adhesion, wear and corrosion performance were not measured directly. The mechanistic discussion of these quantities is therefore limited to literature-supported interpretation of the fractographic observations. Finally, specimen-specific stress and life identifiers for the archived SEM panels were unavailable. Future work should include direct residual-stress measurement, quantitative adhesion testing, fully documented surface-profilometry settings and SEM traceability to individual fatigue specimens.

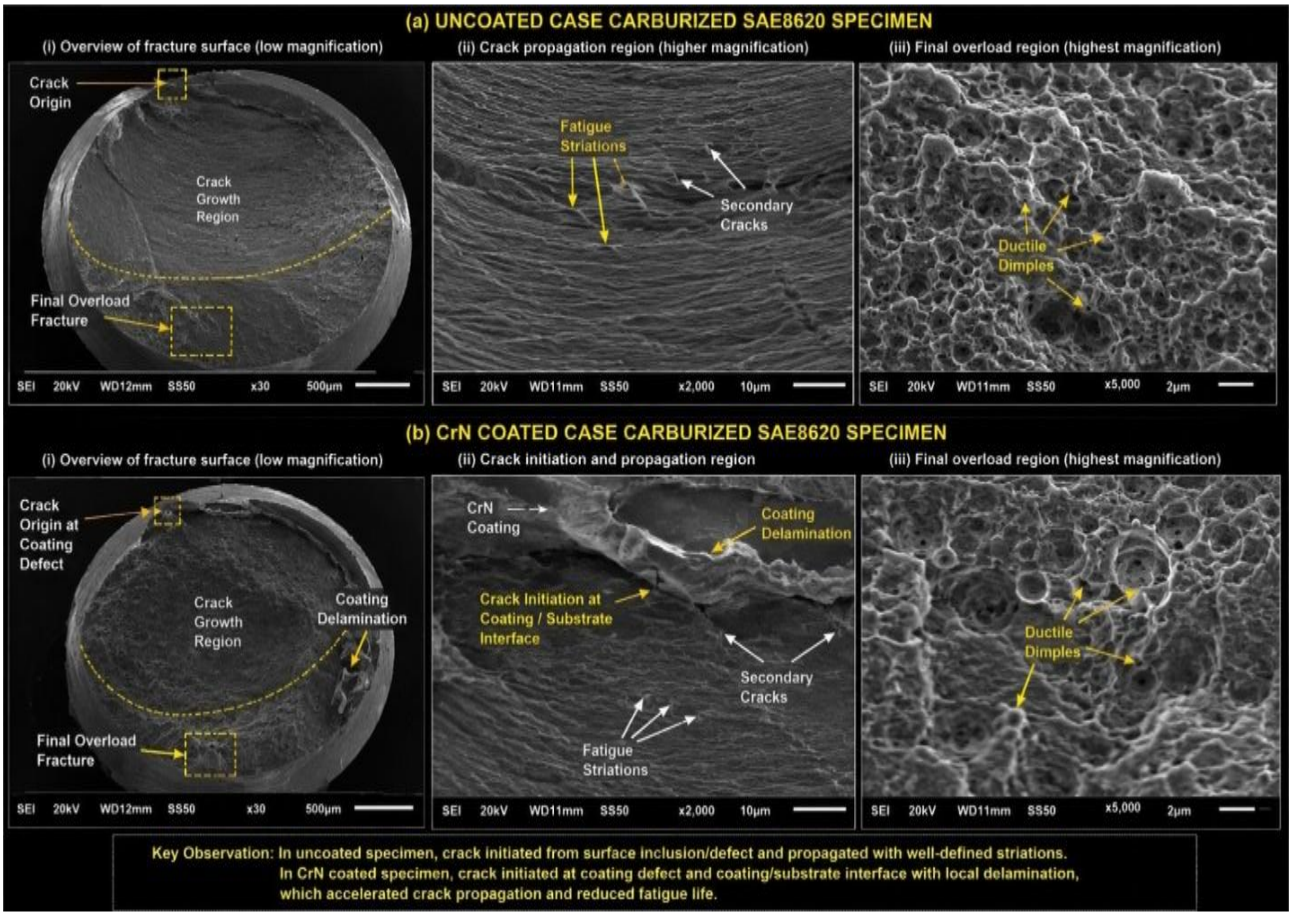

Fig. 4. SEM fractographs of uncoated and CrN-coated case-carburized SAE8620 specimens.

4. CONCLUSION

The influence of a physical vapour deposited chromium nitride (CrN) coating on the fatigue behaviour of case-carburized SAE8620 steel was investigated under four-point rotating bending. Comparisons between coated and uncoated conditions were made using fitted S-N curves because the two series were tested at different stress levels. The following conclusions are drawn from the present experimental results:

1. Case carburization, followed by quenching and tempering produced a hardened surface layer with a hardness of 60–62 HRC, providing a suitable microstructure for fatigue testing.
2. Fatigue life increased with decreasing applied stress for both specimen conditions. Over the overlapping experimentally supported life range, the fitted S-N curve for the CrN-coated condition showed lower fatigue strength at a common life than the fitted curve for the uncoated condition.
3. The separation between the fitted S-N curves increased toward longer lives within the measured range, suggesting a stronger coating influence in the high-cycle region. This trend is consistent with, but does not independently prove, an increased role of coating-associated crack initiation.

4. The mean endurance limits determined using the Dixon–Mood method were 770 MPa for the uncoated specimens and 657.5 MPa for the CrN-coated specimens, corresponding to an approximate 15% reduction in endurance limit after coating.
5. Combining the Basquin fits gives a life-dependent coating knockdown factor, K(N) ≈ 1.33N^-0.032. Within the experimentally investigated range, the predicted fatigue-strength penalty increases from about 1% at 10^4 cycles to about 13% at 5 × 10^5 cycles. No quantitative claim is made at 10^6 cycles because that life lies outside the coated experimental range.
6. SEM examination showed that fatigue cracks in the coated specimens generally initiated at coating defects as well as at the coating/substrate interface, whereas crack initiation in the uncoated specimens occurred mainly from isolated surface discontinuities. Local coating cracking and partial delamination accelerated fatigue crack nucleation.
7. Under the present experimental conditions, the CrN-coated specimens showed lower fatigue resistance. CrN was selected for its established surface-engineering applications, but wear resistance, corrosion resistance, coating adhesion and residual stress were not directly measured in this study; statements concerning these properties are therefore limited to literature-based context and mechanistic interpretation.
8. Benchmarking against a companion study of an identically deposited CrN coating on case-carburized 20MnCr5 steel [14] showed a smaller proportional reduction in endurance limit (5.8%) than the 14.6% reduction found for SAE8620 in the present work. This comparison indicates substrate sensitivity of the coating-associated fatigue penalty, while not establishing the specific microstructural or residual-stress mechanism responsible.

Overall, the study demonstrates that the fatigue response of a hard coating should be evaluated directly for the specific coating/substrate system rather than inferred from its surface-engineering function. For fatigue-critical applications, coating and deposition parameters should be optimized and validated against cyclic-loading requirements.

Statements

CRediT author contribution statement:

B. S. Saini: Conceptualization; Formal Analysis; Visualization; Supervision; Writing-Review and Editing.
Sushil Kumar: Methodology; Investigation; Data Curation; Writing-Original Draft; Resources.

Declaration of conflicting interest:

The authors declare no conflicts of interest.

Funding:

No financial support was obtained for conducting this study.

REFERENCES

[1] "ASM handbook. 1: Properties and selection: irons, steels, and high-performance alloys," 8. print., Materials Park, Ohio: ASM International, 2007, doi: 10.31399/asm.hb.v01.9781627081610.

[2] M. MackAldener and M. Olsson, "Tooth Interior Fatigue Fracture — computational and material aspects," *International Journal of Fatigue*, vol. 23, no. 4, pp. 329–340, Apr. 2001, doi: 10.1016/s0142-1123(00)00099-2.

[3] B. Shaw, "The role of residual stress on the fatigue strength of high performance gearing," *International Journal of Fatigue*, vol. 25, no. 9–11, pp. 1279–1283, Sep. 2003, doi: 10.1016/j.ijfatigue.2003.08.014.

[4] O. Asi, A. Ç. Can, J. Pineault, and M. Belassel, "The effect of high temperature gas carburizing on bending fatigue strength of SAE 8620 steel," *Materials & Design (1980-2015)*, vol. 30, no. 5, pp. 1792–1797, Jul. 2008, doi: 10.1016/j.matdes.2008.07.020.

[5] K. Genel, "Effect of case depth on fatigue performance of AISI 8620 carburized steel," *International Journal of Fatigue*, vol. 21, no. 2, pp. 207–212, Feb. 1999, doi: 10.1016/s0142-1123(98)00061-9.

[6] H. T. S. Ogata, A. S. C. M. D'Oliveira, and P. S. C. P. Da Silva, "Determination of residual stresses in carburized, quenched and tempered AISI 8620 steel," *Materials Science Forum*, vol. 404–407, pp. 197–204, Aug. 2002, doi: 10.4028/www.scientific.net/msf.404-407.197.

[7] O. Asi, A. Ç. Can, J. Pineault, and M. Belassel, "The relationship between case depth and bending fatigue strength of gas carburized SAE 8620 steel," *Surface and Coatings Technology*, vol. 201, no. 12, pp. 5979–5987, Dec. 2006, doi: 10.1016/j.surfcoat.2006.11.006.

[8] R. S. Prasad, D. Mishra, J. Swarnkar, O. Kumawat, M. Pandey, and A. Gupta, "Fatigue analysis of SAE8620: Synergistic effect of thermal treatments and surface roughness," *Advances in Materials and Processing Technologies*, vol. 9, no. 4, pp. 2042–2058, Dec. 2022, doi: 10.1080/2374068x.2022.2152594.

[9] S. Chatterjee, S. Chandrashekhar, and T. S. Sudarshan, "Deposition processes and metal cutting applications of TiN coatings," *Journal of Materials Science*, vol. 27, no. 13, pp. 3409–3423, Jan. 1992, doi: 10.1007/bf01151815.

[10] [S. Baragetti and F. Tordini, "Fatigue and Contact Fatigue Resistance of Thin Hard-Coated Components," *KEM*, vol. 417–418, pp. 801–804, Oct. 2009, doi: 10.4028/www.scientific.net/KEM.417-418.801.

[11] E. S. Puchi-Cabrera, F. MatíNez, I. Herrera, J. A. BerríOs, S. Dixit, and D. Bhat, "On the fatigue behavior of an AISI 316L stainless steel coated with a PVD TiN deposit," *Surface and Coatings Technology*, vol. 182, no. 2–3, pp. 276–286, Apr. 2004, doi: 10.1016/j.surfcoat.2003.07.003.

[12] S. Baragetti, L. Lusvarghi, F. P. Mantini, and F. Tordini, "Fatigue behaviour of notched PVD-Coated titanium components," *Key Engineering Materials*, vol. 348–349, pp. 313–316, Sep. 2007, doi: 10.4028/www.scientific.net/kem.348-349.313.

[13] S. Baragetti and F. Tordini, "A Numerical Study of the Fatigue Behaviour of Notched PVD-coated Ti-6Al-4V," *Structural Durability & Health Monitoring*, vol. 3, no. 03, 2007, doi: 10.3970/sdhm.2007.003.165.

[14] S. Kumar and B. S. Saini, "Effect of CrN PVD coating on the fatigue life of case carburized 20MnCr5 steel," *Journal of Mechanical Science and Technology*, vol. 40, no. 2, pp. 993–996, Feb. 2026, doi: 10.1007/s12206-026-0118-z.

[15] B. S. Saini and V. K. Gupta, "Effect of WC/C PVD coating on fatigue behaviour of case carburized SAE8620 steel," *Surface and Coatings Technology*, vol. 205, no. 2, pp. 511–518, Jul. 2010, doi: 10.1016/j.surfcoat.2010.07.022.

[16] *Metallic Materials—Rotating Bar Bending Fatigue Testing*, ISO 1143:2021, International Organization for Standardization, Geneva, Switzerland, 2021.

[17] B. Navinšek, P. Panjan, and I. Milošev, "Industrial applications of CrN (PVD) coatings, deposited at high and low temperatures," *Surface and Coatings Technology*, vol. 97, no. 1–3, pp. 182–191, Dec. 1997, doi: 10.1016/s0257-8972(97)00393-9.

[18] G. Wang, Y. Jiang, X. Wang, and C. Guo, "Review on the mechanical properties of CR-N coatings prepared by physical vapor deposition," *Coatings*, vol. 16, no. 1, p. 9, Dec. 2025, doi: 10.3390/coatings16010009.

[19] O. Hajizad, A. Kumar, Z. Li, R. H. Petrov, J. Sietsma, and R. Dollevoet, "Influence of microstructure on mechanical properties of bainitic steels in railway applications," *Metals*, vol. 9, no. 7, p. 778, Jul. 2019, doi: 10.3390/met9070778.

[20] *Standard Practice for Statistical Analysis of Linear or Linearized Stress-Life (S-N) and Strain-Life (ε-N) Fatigue Data*, ASTM E739-10(2015), ASTM International, West Conshohocken, PA, USA, 2015.

[21] W. J. Dixon and A. M. Mood, "A method for obtaining and analyzing sensitivity data," *Journal of the American Statistical Association*, vol. 43, no. 241, pp. 109–126, Mar. 1948, doi: 10.1080/01621459.1948.10483254.

Nomenclature

S	applied bending stress amplitude (MPa)
N	number of cycles to failure
N_f	average fatigue life at a given stress level (cycles)
σ	standard deviation of fatigue life or of the estimated endurance limit (MPa or cycles, as noted)
μ_s	standard deviation of fatigue life or of the estimated endurance limit (MPa or cycles, as noted)
d	stress increment used in the staircase fatigue test (MPa)
k	stress-level index in the Dixon–Mood staircase analysis
$n_{DM,k}$	number of events (runouts or failures, as defined) at staircase level k
A_{DM}, B_{DM}	first and second statistical moments used in the Dixon–Mood calculation